PI Current Controller Design for DC Drive System using 4- Quadrant DC-DC Converter and 3- Phase Rectifier

MUSTAFA SAAD, KHALED MUSTAFA
Control Engineering Department,
College of Electronic Technology Bani Walid,
Bani Walid,
LIBYA

Abstract: - DC Motors is considered one of the important machines in control systems such as industrial robots, vehicles, and process control. Current control of a DC drive is very desirable because by controlling the current, the torque is controlled. Moreover, current control can be used to prevent large damaging armature currents during start-up. A good current loop is very important when setting up a DC drive. When the control of the current loop is good, the steady state motor current should respond exactly with the reference current, and the transient response to the step change in the reference current should be fast and well-damped. This paper presents two different types of current controller converters that are commonly used in DC motor drives. The first converter is a 4-quadratic switch-mode DC-DC converter, while the second controller is a 3-phase controller rectifier. Both current converters were simulated using Matlab Simulink, where a PI current controller for the inner loop current control DC motor controls these converters. The PI controller was designed based on the Bode plot frequency response method. In this research, the design procedure was based on the small signal model and then, verified using a large signal model. The simulation result showed that the performance using a 4-quadrant DC-DC converter gave better performance than a 3-phase rectifier.

Key-Words: - DC Motor Drive, 4-quadrant Switch Mode, 3-phase Rectifier, Closed Loop, PI Controller

Received: March 27, 2023. Revised: January 7, 2024. Accepted: February 22, 2024. Published: April 2, 2024.

1 Introduction

DC motors were used last time. The DC network was the first developed electric network and was constructed to work on the DC electric network. Nowadays, the majority of industry-installed motors consist of AC motors, due to their high-speed operation and their smaller volume and weight. Additionally, AC motors, due to their construction, require lighter maintenance and are cheaper compared to DC motors. However, DC motors are still used for several reasons, including, wide speed range, starting and accelerating torques more than 400% of their rated values, good speed regulation, and simpler and cheaper control systems. Their main applications include the manufacture of pulp, paper, and paperboard, propulsion of electric vehicles, textile industries, and public transportation, such as subway and trolley systems. Modern DC motor drives utilize power electronic devices and are subdivided into chopper-fed and controlled thyristor-fed drives, [1]. The classification of DC motor drives can be done according to the type of the utilized converter, which controls the speed and the torque of the DC motor, [2]. Nowadays, controlling DC motors with high performance requires the use of DC-to-DC converters, [3], [4], [5], [6], [7], [8], [9], [10], [11], [12], [13], [14].

2 Four Quadrant Converter

The developed model for the two-quadrant converter can be used as a building block in developing the model for the four-quadrant converter, [15]. As illustrated in Figure 1, the four-quadrant converter is composed of two legs, A and B, with each leg similar to the other.

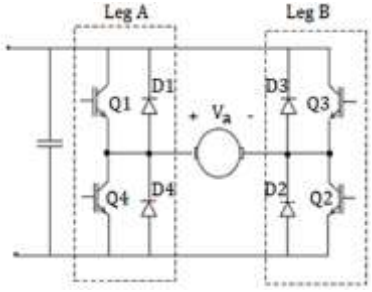

Fig. 1: A developed model for a four-quadrant converter

The instantaneous voltage Va can be made either equals.

For positive current
$V_a = V_{dc}$ when Q1 and Q2 are ON
$V_a = -V_{dc}$ when D3 and D4 are ON
$V_a = 0$ when current freewheels through Q & D.

For negative current
Va = Vdc when D1 and D2 are ON
Va = -Vdc when Q3 and Q4 are ON
Va = 0 when current freewheels through Q & D.

In the four-quadrant converter, two switching schemes are normally employed which are the bipolar switching scheme, and the unipolar switching scheme, [15].

2.1 Bipolar Switching Scheme

Leg A and Leg B obtained the switching signals from the same control signal. This implies that switching Leg A and Leg B are always complements. In a forward-breaking mode where the average voltage V_a is positive and smaller than the back emf of the armature, the current will flow through D1 and D2 when $V_a = V_{dc}$ and will flow through Q3 and Q4 when $V_a = -V_{dc}$. By using the comparison between the control signal and triangular waveform as shown in Figure 2, the waveform q and $\bar{q}$ were obtained as shown in Figure 3.

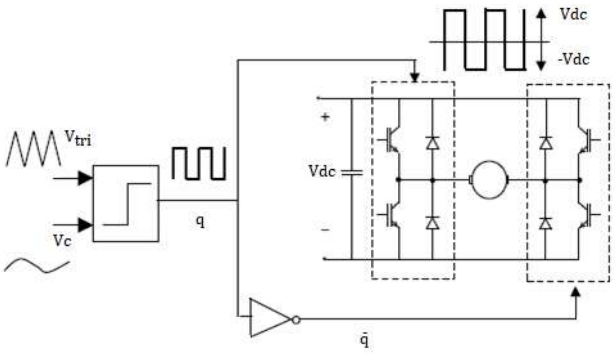

Fig. 2: The control signal, V_c, and triangular waveform, V_{tri} in a bipolar switching scheme.

The waveforms q and $\bar{q}$ were obtained from the following rules:

$$q = \begin{cases} 0 & V_c < 2V_{tri} \\ 1 & V_c > 2V_{tri} \end{cases} \quad and \quad \bar{q} = -q$$

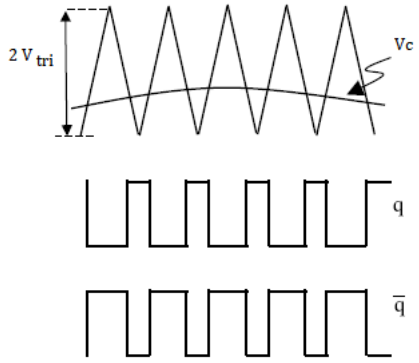

Fig. 3: Waveforms for q and $\bar{q}$ after a comparison between V_c and V_{tri}

2.2 Unipolar Switching Scheme

In the unipolar switching scheme, the switching signal for Leg B is obtained from the inverse of the control signal for Leg A. Figure 4 illustrates the unipolar switching scheme and Figure 5 shows the resultant waveform q and $\bar{q}$.

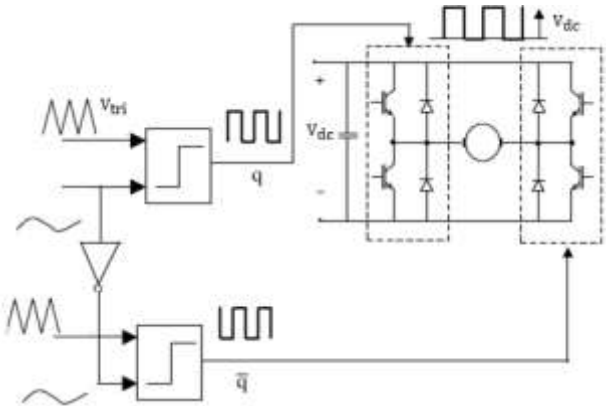

Fig. 4: The control signals V_c and triangular waveform, V_{tri} in a unipolar switching scheme

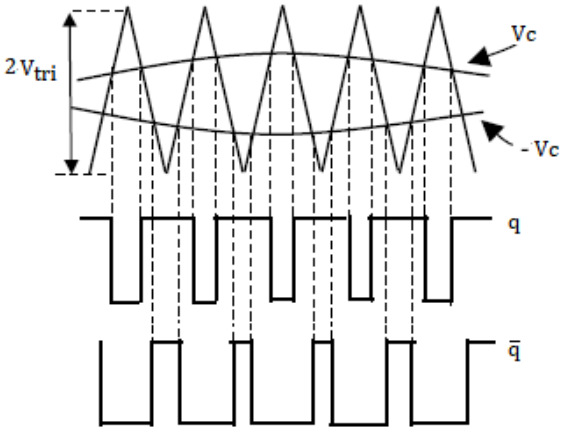

Fig. 5: The resultant waveform in a unipolar switching scheme

The waveforms q and $\bar{q}$ were obtained from the following rules:

$$q = \begin{cases} 0 & V_c < 2V_{tri} \\ 1 & V_c > 2V_{tri} \end{cases} \quad and \quad \bar{q} = q$$

$$= \begin{cases} 0 & -V_c < 2V_{tri} \\ 1 & -V_c > 2V_{tri} \end{cases}$$

The relationship between $V_a(s)$ and $V_c(s)$ for both Bipolar and Unipolar is

$$\frac{V_a(s)}{V_c(s)} = \frac{V_{dc}}{V_{tri}} \quad (1)$$

3 Three-Phase Controlled Rectifier

The steady state and dynamic behavior of the controlled rectifier are highly nonlinear which can be described by a nonlinear differential equation. Thus, to simplify the controller design for the controlled rectifier, an average or linearized model is used. However, tile approximation is only valid if the bandwidth of the control loop is much lower than the sampling frequency to ensure a continuous current mode. Figure 6 shows the closed loop AC-DC controlled rectifier.

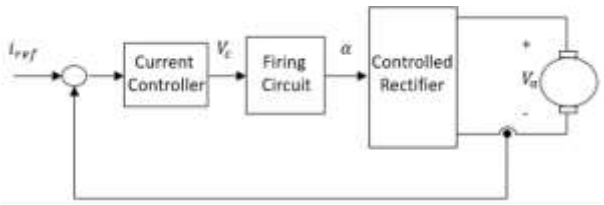

Fig. 6: Close loop AC-DC controlled rectifier

The relationship between the average voltage and the firing angle of a 3-phase controlled rectifier is given by [16]

$$V_a = \frac{3V_m}{\pi} \cos\alpha \quad (2)$$

$V_{rms}(line - line) = 141v$, f=50Hz and with α=0.

$$V_{rms} = \frac{V_m}{\sqrt{2}} \quad (3)$$

$$V_m = 141 \times \sqrt{2} = 199.4\ v$$

$$V_a = 190.416\ v$$

4 Proportional Integral Controller

The proportional term and the integral term are combined to form the PI controller. The PI controller has a beneficiary effect on the steady-state error since ti increases the system type of the system by one. In general, the proportional term affects the system's stability. Where too high proportional gain gives oscillation or an unstable system. The integral term is used to eliminate the steady-state error. However, setting the integral gain too high is to invite oscillation, instability, and integrator windup or actuator saturation. The transfer function of the PI controller is

$$G_c(s) = \frac{U(s)}{E(s)} = \frac{K_i + K_P s}{s} = \frac{K_i(1 + \frac{s}{K_i/K_P})}{s} \quad (4)$$

5 Simulation Results and Discussions

In this section, the simulation is done using Matlab Simulink to see the characteristics of the two current controller converters. Firstly, the 4-quadratic unipolar converter has been done, then the 3-phase controlled rectifier. Both current controllers were simulated using the linear small signal model and large signal model. Table 1 shows the system parameters.

Table 1. System parameters

Component	Value
V_{dc}	200 v
V_{tri}	5 v
f_{tri}	5000 Hz
N_{rated}	1313 rpm
V_{rated}	120 v
R_a	0.8 Ω
L_a	103 mH
$K_T = K_E$	0.764 vs/rad
J	2 Kg.m^2
B	0.06 N.m.s
f	50 Hz

5.1 Simulation Result using 4-Quadrant Converter

Use the parameters in Table 1 to design a small signal model, which is shown in Figure 7. In this research, the PID controller simulation block is used and to use the PI controller the derivative term is set to zero. Figure 8, and Figure 9 shows the Bode plot and Pole Zero location of the open loop gain with K_p=1 and K_i=0.

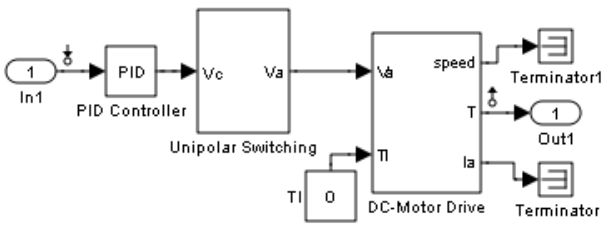

Fig. 7: Small signal model for 4-quadratic converter

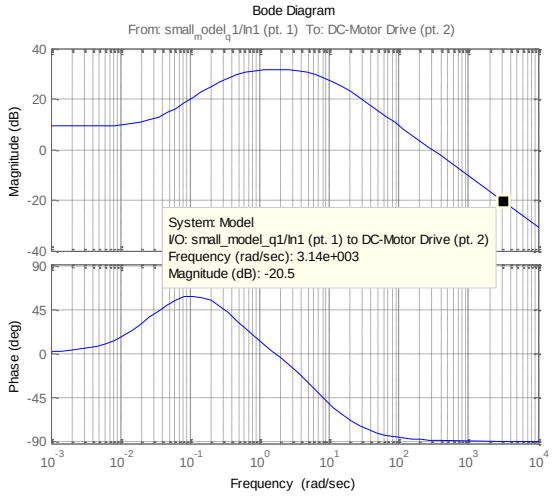

Fig. 8: Bode plot of a small signal model for a 4-quadratic converter

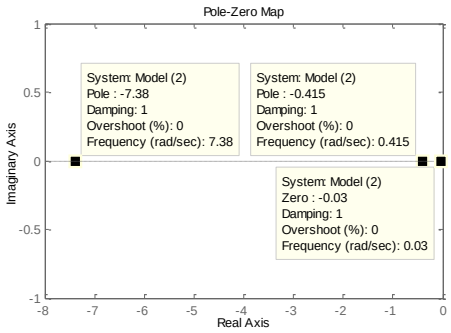

Fig. 9: Pole zero location of a small signal model

From Figure 9, the system has two poles at 0.415 and 7.38. If the zero crossover frequency of the PI controller is set at 4 rad/sec, then K_i /K_P=4 rad/sec. and if the DC gain is set to unity (by setting K_i =1), then K_P must be set to 0.25, the Bode plot for this condition is shown in Figure 10.

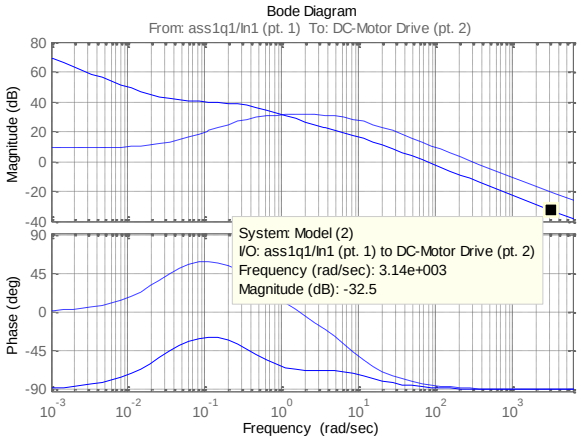

Fig. 10: Open loop gain with K_i =1 and K_p =0.25 (solid line) for 4-quadratic converter

From Figure 10 it can be seen that the crossover frequency or the bandwidth is too low. To increase the bandwidth while maintaining the zero at 4 rad/sec, the value of K_i needs to be increased. At the same time, K_i needs to be changed accordingly so that the zero at 4 rad/sec is maintained. Since the bandwidth is 500 Hz = 3.14×10^3 rad/sec. the magnitude curve has to be raised by 32.5 dB.

$$20 \log K_i = 32.5$$
$$K_i = 10^{(32.5/20)} = 42.169$$
$$K_P = 10.542$$

The new controller gains K_i and K_P are used in the simulation diagram and the Bode plot is obtained as shown in Figure 11.

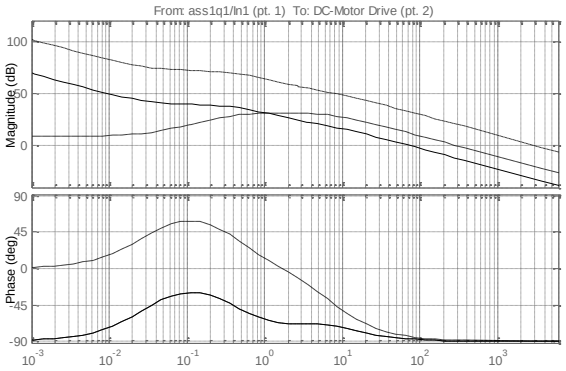

Fig. 11: Bode plot for K_i = 42.169 & K_p = 10.542 (dash-dotted)

From Figure 11, the magnitude is nearly zero dB and the phase margin is greater than 65°, then we take the computed values of K_i and K_p to be implemented into the large signal simulation as in Figure 12.

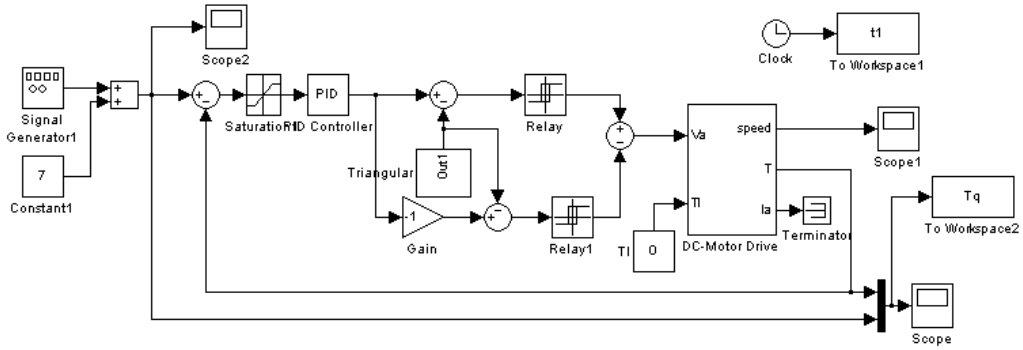

Fig. 12: Large signal model for closed-loop current control for 4-quadratic converter

5.2 Simulation Result using 3-Phase Controlled Rectifier

The linear small signal model for the 3-phase controlled rectifier is shown in Figure 13.

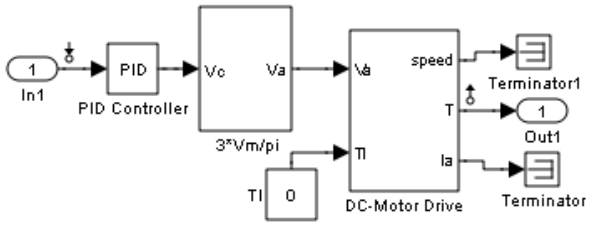

Fig. 13: Small signal model for 3-phase converter

It is desired that the bandwidth of the current controlled converter be 30 Hz. The poles are at the same location because we use the same system so we use the same pole-zero location as in Figure 9. Therefore, Figure 14 shows the Bode plot of the open loop gain with K_p=1 and K_i=0.

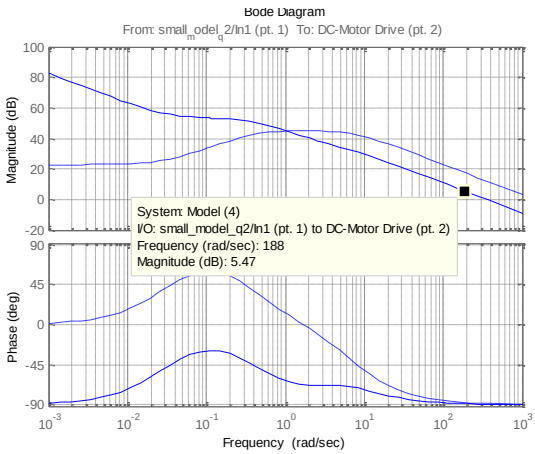

Fig. 14: Bode plot of a small signal model for a 3-phase converter

Same as 4-quadratic. K_i =1 and K_p =0.25. The Bode plot for this condition is shown in Figure 15.

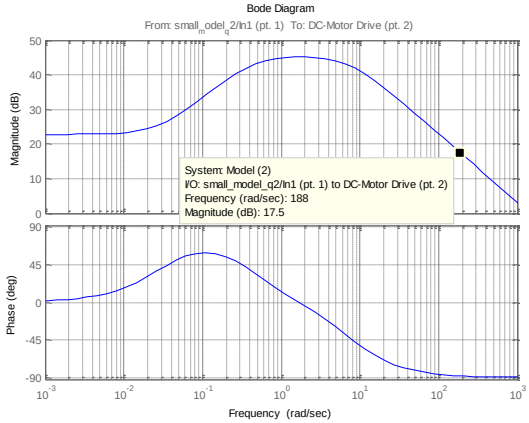

Fig. 15: Open loop gain with K_i =1 and K_p =0.25 (solid line) for 3-phase converter

From Figure 15 it can be seen that the crossover frequency or the bandwidth is too high. To decrease the bandwidth while maintaining the zero at 4 rad/sec, the value of K_i needs to be decreased. At the same time, K_i needs to be changed accordingly so that the zero at 4 rad/sec is maintained. Since the bandwidth is 30 Hz = 188.49 rad/sec, we need to decrease the gain by 5.47 dB.

$$20 \log K_i = -5.47$$
$$K_i = 0.5327 \quad \text{and} \quad K_P = 0.1331$$

By putting the new values of K_i and K_P in the simulation diagram, then the Bode plot of the new values is shown in Figure 16.

From Figure 16, the magnitude is nearly zero dB and the phase margin is greater than 65°, then we take the computed values of K_i and K_p to be implemented into the large signal simulation as in Figure 17.

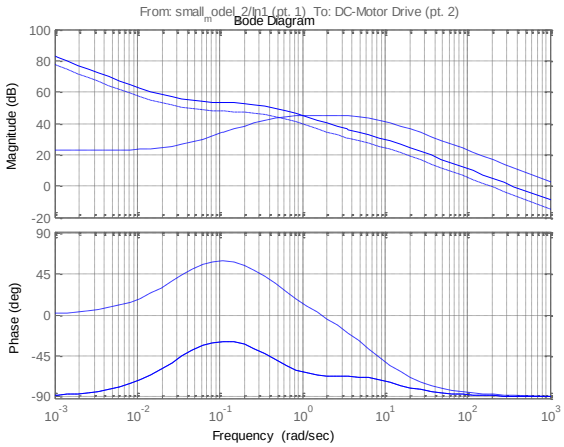

Fig. 16: Bode plot for $K_i = 0.5327$ & $K_p = 0.1331$ (dash-dotted) for 3-phase converter

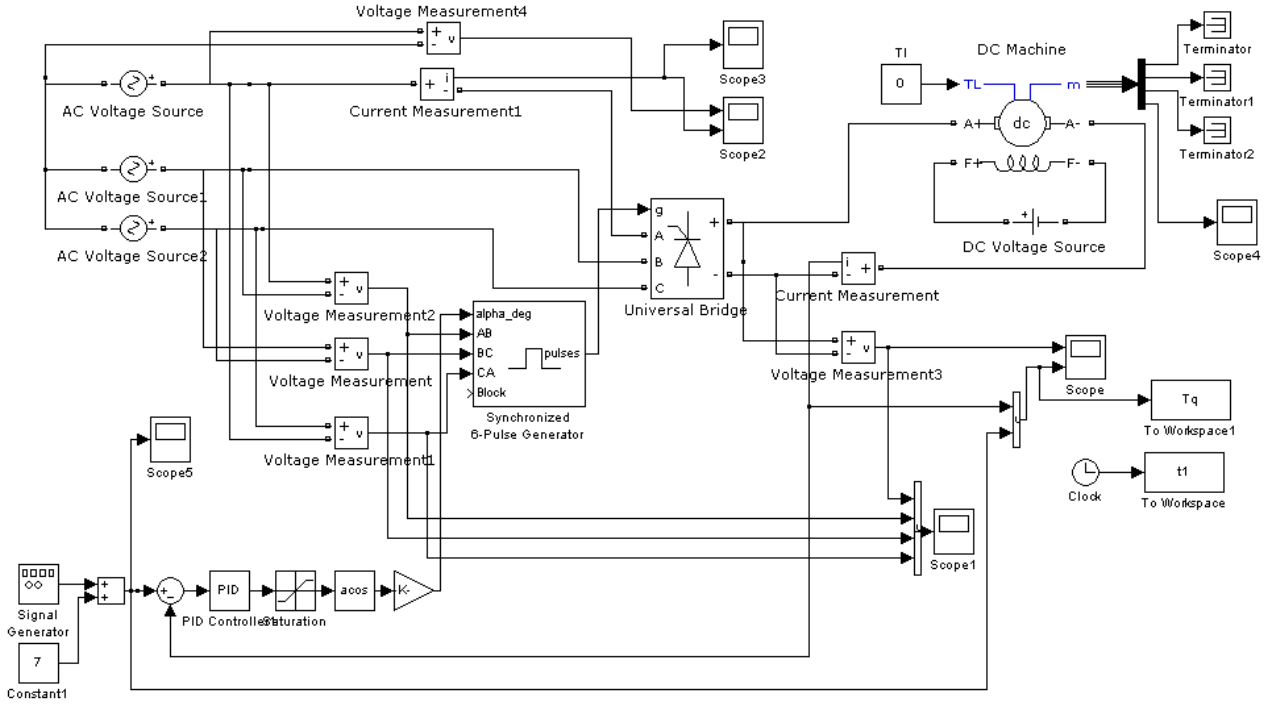

Fig. 17: Large signal model for closed-loop current control for 3-phase converter

Figure 18 and Figure 19 show the torque response for the 4-quadratic converter and 3-phase converter respectively.

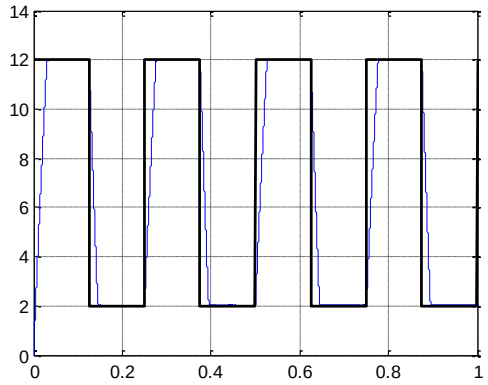

Fig. 18: Torque response for 4-quadratic converter

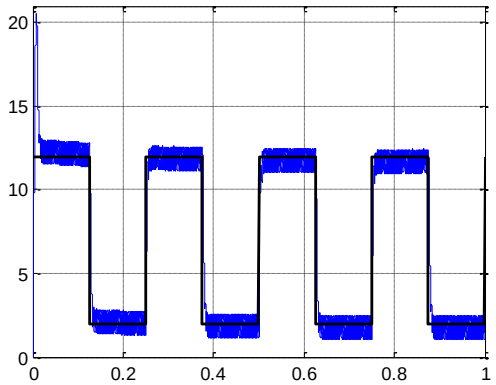

Fig. 19: Torque response for 3-phase converter

It can be seen from the simulation results that the 3-phase converter produces more ripples compared to that of the switch-mode 4-quadratic converter, which is almost not observable.

6 Conclusion

In this research, two different control models were designed by using a 4-quadrant DC-DC converter and a 3-phase rectifier to control the DC motor drive in Matlab Simulink software. The PI controller parameters have been designed based on the open loop frequency response technique using a small signal model, then used in a large signal model. From the simulation results, it can be concluded that the 4-quadratic converter has a faster response with zero overshoot and zero steady-state error. In addition, it tracked the reference signal almost immediately. While the 3-phase controlled rectifier has low control bandwidth and high-frequency current ripple.

References:

[1] D. A. Barkas, G. C. Ioannidis, C. S. Psomopoulos, S. D. Kaminaris, and G. A. Vokas, Brushed DC Motor Drives for Industrial and Automobile Applications with Emphasis on Control Techniques: *A Comprehensive Review, Electronics,* Vol. 9, No. 6, 2020 pp. 887.

[2] D. W. Hart, *Introduction to Power Electronics*. Prentice Hall, 1997.

[3] C. C. C. Chan, K.T, A new zero-voltage-switching dc/dc boost converter, *IEEE Trans. Aerosp. Electron. Syst.*, vol. 29, No. 1, pp. 125-134, 1993, doi: 10.1109/7.249118.

[4] C. C. a. C. F. C. Chong, "A quasi-resonant converter-fed DC drive system," presented at the *Fifth European Conference on Power Electronics and Applications,* Brighton, UK, 1993.

[5] G. H. a. F. C. Lee, Soft-switching techniques in PWM converters, *IEEE Transactions on Industrial Electronics*, Vol. 42, No. 6, pp. 595-603, 1995, doi: 10.1109/41.475500.

[6] F. L. J. Luo, L. . Proc., Two-quadrant DC/DC Soft-switching Converter, *presented at the Proc. IEEE Power Electron. Spec. Conf*, 2000.

[7] T. W. Ching, Soft-switching converters for electric vehicle propulsion, *J. Asian Electr. Veh.*, Vol. 5, pp. 1019-1026, 2007.

[8] K. T. Chau, T. W. Ching, and C. C. Chan, A new two-quadrant zero-Voltage transition converter for DC motor drives, *International Journal of Electronics*, Vol. 86, No. 2, pp. 217-231.

[9] T. W. Ching, Four-quadrant zero-Voltage-transition converter-fed DC motor drives for electric propulsion, *J. Asian Electr. Veh.*, Vol. 3, pp. 651-656, 2005.

[10] T. W. Ching, Four-quadrant zero-current-transition converter-fed DC motor drives for Electric Propulsion, *J. Asian Electr. Veh.*, Vol. 4, pp. 911-918, 2006.

[11] E. Grassi and K. Tsakalis, PID controller tuning by frequency loop-shaping: application to diffusion furnace temperature control, *IEEE Transactions on Control Systems Technology,* Vol. 8, No. 5, pp. 842-847, 2000, doi: 10.1109/87.865857.

[12] F. Loucif, DC Motor Speed Control using PID Controller, *presented at the International Conference on Control, Automation and Systems KINTEX, Gyeonggi-Do, Korea*, 2005.

[13] G. C. K. Ioannidis, S.D. Psomopoulos, C.S. Tsiolis, S. Pachos, P. Villiotis, I. Malatestas, P., DC Motor Drive Applying Conventional and Fuzzy Based PI Control Techniques, *JARR* Vol. xv, pp. 1-10, 2015.

[14] B. P. Singh, S. Pandey, A.S. Sinha, S.K., Intelligent PI Controller for Speed Control of D.C. Motor, *Int. J. Electron. Eng. Res.* Vol. 2, pp. 87-100, 2010.

[15] J. Wang, W. G. Dunford, and K. Mauch, Some novel four-quadrant DC-DC converters, *in PESC 98 Record. 29th Annual IEEE Power Electronics Specialists Conference* 1998, Vol. 2, pp. 1775-1782.

[16] B. W. Williams, *Power Electronics: Devices, Drivers, Applications and Passive Components*, Subsequent ed. McGraw-Hill, 1992.

Contribution of Individual Authors to the Creation of a Scientific Article (Ghostwriting Policy)

- Mustafa Saad carried out the simulation and the controller design.
- Mustafa Saad and Khaled Mustafa have organized and executed the research of Section 5.
- Khaled Mustafa was responsible for the text writing.

Sources of Funding for Research Presented in a Scientific Article or Scientific Article Itself

No funding was received for conducting this study.

Conflict of Interest

The authors have no conflicts of interest to declare.